Progress In Electromagnetics Research, PIER 98, 175–190, 2009

SIMULATION OF TIME MODULATED LINEAR ANTENNA ARRAYS USING THE FDTD METHOD

S. W. Yang, Y. K. Chen, and Z. P. Nie

Department of Microwave Engineering
School of Electronic Engineering
University of Electronic Science and Technology of China (UESTC)
Chengdu 610054, China

Abstract—Time modulated linear antenna arrays consisting of printed dipoles above a ground plane are simulated using the finite-difference time-domain (FDTD) method. The FDTD method brings great convenience to the investigation of the time domain responses of the time modulated arrays. In conjunction with the near-to-far field transformation in time domain, the far-field transient response can be computed to explain the physical essence of different time sequences. By employing the discrete Fourier Transform (DFT) and the frequency domain near-to-far field transformation, the radiation patterns at the frequencies of interest are obtained and are compared with the measured results. Simulation results show that the FDTD method is an effective and accurate approach for the full-wave simulation of time modulated antenna arrays.

1. INTRODUCTION

The amplitude excitations in conventional antenna arrays usually have large dynamic range ratios to obtain low or ultra-low sidelobe levels (SLLs). However, such antenna arrays are usually rather difficult and expensive to be realized in practice. Moreover, excitations in conventional antenna arrays are usually much influenced by various errors, such as the systematic errors and random errors, etc. [1]. On the other hand, the time modulated array proposed by Kummer [1] is a good candidate to meet these kinds of challenges. Recently, a substantial amount of studies have been carried out on time modulated antenna arrays, including synthesis of radiation patterns with low/ultra-low SLLs [2–4], synthesis of shaped beam patterns [5],

Corresponding author: S. W. Yang (swnyang@uestc.edu.cn).

sidebands suppression using optimization algorithm [2, 6], studies on various time sequences [3, 6–9], mutual coupling compensation in time modulated antenna arrays [10], and the full-wave simulation of time modulated antenna arrays in frequency domain [11].

Despite the promising results obtained in the aforementioned studies, none of the studies were on the time domain analysis of time modulated arrays. In order to obtain a full understanding of the time modulated arrays, an investigation in time domain is of great necessity. In fact, the time modulated array possesses an inherent nature of periodic variation with respect to time, thus a time domain approach should be advantageous in analyzing the time modulated arrays. On the other hand, the FDTD method, firstly proposed by Yee [12], is one of the most predominate full-wave simulation methods in the analysis of antenna and antenna arrays [13, 14]. It provides a general formulation to problems with complicated structure and inhomogeneous material in the computation domain. Furthermore, it outperforms any other frequency domain methods in that it can be used to obtain the wideband frequency responses and time domain far-field waveforms using only one single simulation.

In this paper, the FDTD method is applied to the analysis of time modulated linear arrays with two types of time sequences, namely, the variable aperture sizes (VAS) [7] and the bidirectional phase center motion (BPCM) [9]. The numerical results well explained the inherent physical essence of the two types of time sequences in time modulated antenna arrays. The radiation patterns obtained over the frequencies of interest are in good agreement with published measurement results, thus validating the effectiveness of the proposed FDTD approach in the simulation of the time modulated antenna arrays.

2. THEORY OF TIME MODULATED ANTENNA ARRAYS

Consider an N-element linear array of equally spaced parallel dipoles, each element is controlled by a high speed RF switch and is excited with a complex excitation $A_k\,(k = 1, 2, \ldots, N)$. When a plane wave of frequency f_0 is incident at an angle θ with respect to the normal of the array, the output of the array is given by:

$$E(\theta, \varphi, t) = e_0(\theta, \varphi) e^{j2\pi f_0 t} \sum_{k=1}^{N} A_k U_k(t) e^{j(k-1)\beta d \sin\theta} \tag{1}$$

where $e_0(\theta, \varphi)$ is the common radiation pattern of each dipole, and $U_k(t)$ refers to the periodic on-off switching time sequence function for

the kth element. Two types of time sequence functions are discussed in this paper. For the time modulated linear arrays with VAS, the kth element is switched on for an interval of τ_k within one pulse repetition period T_p. Consequently, $U_k(t)$ can be expressed as:

$$U_k(t) = \begin{cases} 1 & 0 \le t \le \tau_k \\ 0 & \text{otherwise} \end{cases} \tag{2}$$

By decomposing (1) into Fourier series with different frequency components separated by $prf = 1/T_p$, the response of the far-field pattern in the spatial and time domain is given by:

$$E(\theta, \varphi, t) = e_0(\theta, \varphi) e^{j2\pi f_0 t} \sum_{m=-\infty}^{+\infty} \sum_{k=1}^{N} a_{mk} e^{j(k-1)\beta d \sin\theta} e^{j2\pi m \cdot prf \cdot t} \tag{3}$$

where the excitation for the mth harmonic on the kth element is integrated as:

$$a_{mk} = \frac{A_k \tau_k}{T_p} \cdot \frac{\sin\left[\pi m \tau_k \cdot prf\right]}{\pi m \tau_k \cdot prf} \cdot e^{-j\pi m \tau_k \cdot prf} \tag{4}$$

Similarly, when the linear array is modulated with a continuous (C-Scheme) BPCM in [9], the time switching function can be expressed as:

$$U_1(t) = \begin{cases} 1 & 0 \le t \le \tau \\ 0 & \text{otherwise} \end{cases} \tag{5}$$

$$U_k(t) = \begin{cases} 1 & t_{1k} \le t \le t_{2k} \\ 1 & t_{3k} \le t \le t_{4k} \\ 0 & \text{otherwise} \end{cases} \quad (1 < k \le N - M) \tag{6}$$

$$U_k(t) = \begin{cases} 1 & t'_{1k} \le t \le t'_{2k} \\ 0 & \text{otherwise} \end{cases} \quad (N - M < k \le N) \tag{7}$$

where M is the number of elements being switched to the on-state at any time instants, $\tau, t_{1k}, t_{2k}, t_{3k}, t_{4k}, t'_{1k}, t'_{2k}$ are the "on" and "off" time switching instants, and more details on them are given in [9]. The corresponding complex excitation a_{mk} for the mth harmonic on the kth element is also presented in [9].

According to (3), we can find that undesired radiation does exist for each frequency component m, whose amplitude level is controlled by the Fourier coefficient a_{mk}. Although the response of the far-field pattern in the spatial and frequency domain has been investigated either by analytical method [7, 9] or by full-wave simulations in frequency domain [11], the results obtained by the FDTD method will also be presented for comparison in Section 4. It is necessary to point out that the transmitted signal is assumed to be a rectangular pulse

in this study, and the C-Scheme is applied both for the time sequences of BPCM and VAS, i.e., the pulse repetition period T_p equals to the rectangular pulse width T, where $T = 1/B$ and B is the passband of the radar or other system receiver.

3. FDTD MODEL OF TIME MODULATED ANTENNA ARRAYS

The time modulated linear array to be modeled in FDTD comprises of 16 printed dipoles above a perfect conducting ground of finite sizes, as illustrated in Figure 1. The dipoles are parallel to the y-axis and are arrayed along the x-axis, with a $\lambda/2$ spacing at the operating frequency f_0. The origin of the coordinate system is supposed to be located at the geometrical center of the linear array.

The FDTD approach requires a free space surrounding the array, which is divided into a number of rectangular bricks in the three-dimensional space. As to the radiation problem considered in this paper, the computational domain should be truncated due to the limited computer resources. Therefore, the perfectly matched layer (PML) developed by Berenger [15, 16] is implemented to truncate the computational domain from open space to make the actual computation possible.

Equation (2) shows that the time modulated array in this paper is excited with rectangular pulses. Undoubtedly, the rectangular pulse in experiment cannot be an ideal rectangular shape because of the rising and falling edges. Thus, the rising and falling edges of the ideal rectangular pulse should be modified. Another benefit from this practical consideration is that the shock waves excited by an ideal rectangular pulse can be avoided in the FDTD simulation. In order to simulate the rising and falling edges in a rectangular pulse, the

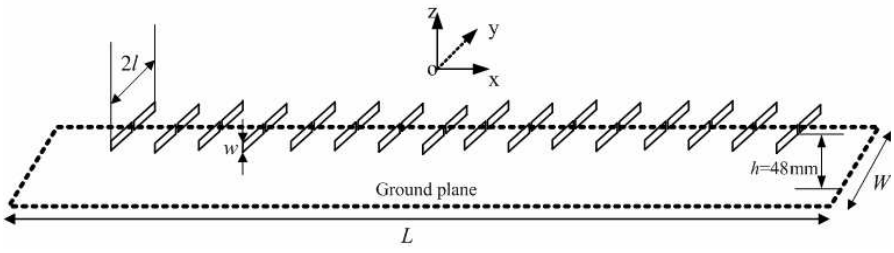

Figure 1. Configuration of the time modulated linear array.

Gaussian pulse is a suitable candidate in this case, which has the following form:

$$V(n\Delta t) = e^{-(n\Delta t - t_0)^2/T^2} \tag{8}$$

where Δt is the time increment in the FDTD method, T is the pulse half-duration at the $1/e$ point, and it determines the Gaussian width. t_0 governs the rising or falling time of the pulse. The peak value of the Gaussian appeared at $n\Delta = t_0$. By applying the Fourier transform to the Gaussian pulse (8), we have

$$G(f) = T\sqrt{\pi}\exp\left(-j2\pi f t_0 - \pi^2 f^2 T^2\right) \tag{9}$$

In this paper, the rising and falling edges of the rectangular pulse are approximated by their counterparts in the Gaussian pulse. By choosing the rising or falling time t_0 and the pulse half-duration time T (defined in term of the $1/e$ point) properly, the rising and falling time of the ideal rectangular pulse can be modified efficiently. Generally, the half-duration time of the Gaussian pulse can be chose to be relatively larger than $\sqrt{\pi}T$. Here, we chose the half-duration width of the Gaussian pulse to be $3/\sqrt{2}T$, and the rising time (or falling time) is set to be as half the width of the pulse in time, i.e., $t_0 = 3T/\sqrt{2}$. In this case, the magnitude at the rising edge is about 1.11% of the peak value. For the sake of obtaining the far-field pattern in a broad range of frequencies, the sine wave modulated rectangular pulse is adopted to stimulate the excitation between the two arms of each dipole. Shown in Figure 2 are the rectangular pulse with the rising and falling edges and the sine wave modulated rectangular pulse in free space within one pulse repetition period T_p. As can be seen, by setting the proper value of t_0 and T, the rising and falling edges in rectangular pulse can be well approximated.

Two types of near-to-far-field transformation, namely, transformation carried out in the time domain and frequency domain, are incorporated into the FDTD algorithm to obtain the time response and the radiation pattern in the far zone. Similar to other electromagnetic

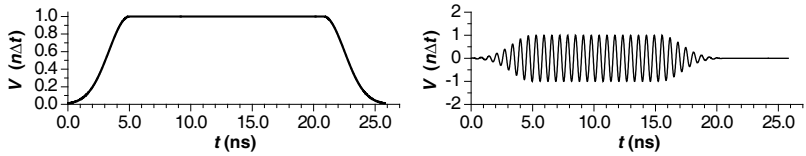

Figure 2. Rectangular pulse and modulated rectangular pulse. (a) Rectangular pulse with the rising and falling edges of Gaussian pulse; (b) the sine wave modulated rectangular pulse.

problems involved with the FDTD method, the time modulated array is enclosed in a closed Huygens's surface, which is chosen to be a cube inside the PML ABCs. A brief review of the two methods is presented in the following.

In the time domain near-to-far-field transformation [17, 18], the equivalent currents at each time step are computed from the fields on the Huygens's surface. The contributions of the equivalent currents from each cell on the surface are put into corresponding time bins, thus the time domain far fields obtained. In the case where the radiation patterns or other frequency dependent parameters over a broadband of frequencies are required, the Fourier transform can be applied to obtain the results in frequency domain. However, if frequency domain far-field radiations over all the elevation angles are computed through this approach, the FDTD simulation slows down significantly as expected. Moreover, storing the entire time domain signature at all the observation directions would pose a heavy burden on the memory requirements. Thus, in this paper the time domain signature is only computed at a few angles to mitigate the burden on computer resource. Apparently, a pitfall inherent in this method is that the far-field radiations at the ignored directions can not be given.

Although a great deal of information about the response of the far-field radiations has been lost in the time domain transformation, the near-to-far-field transformation in frequency domain [19–21] can well make up its counterpart in time domain. In the time modulated arrays, only spatial responses at the center frequency and several low order sidebands are of interest, thus the single-frequency near-to-far-field transformation [13] is expected to be a well-suited alternative to the time domain transformation when the far-field pattern responses at all the directions are desired. Thus, the computational complexity in the time domain transformation can be avoided for the calculation of the far-field radiations. In the single-frequency near-to-far-field transformation, the electric and magnetic fields are monitored over the Huygens's surface, and then either a Discrete Fourier Transform (DFT) or a Fast Fourier Transform (FFT) is applied to obtain the coefficients of the fields at the desired frequencies. For the ease of implementation and the use of an arbitrary number of samples, DFT is generally preferred. The DFT based transformation from the time domain to the frequency domain is given by

$$\mathbf{E}(k\Delta f, \mathbf{r}) = \Delta t \sum_{n=0}^{N-1} \mathbf{E}(n\Delta t, \mathbf{r}) \exp\left\{-\frac{j2\pi kn}{N}\right\}, \quad (k = 0, 1, 2, \ldots, N) \quad (10)$$

Since only the Fourier coefficients are stored in this scheme, the DFT above needs no much of extra memory storage, and the memory

requirements are much smaller than that needed in the time domain near-to-far-field transformation. Additionally, running of the DFT can be carried out simultaneously with the time marching in the FDTD algorithm, thus the computational complexity of the DFT is far less than that required in the original FDTD. Therefore, the efficiency of the primitive FDTD algorithm is affected little when such technique is employed. Once the prefixed time steps runs out, the frequency domain equivalent currents on the Huygens's surface are computed through the DFT. Consequently, radiation patterns at the desired frequencies can be easily obtained with these equivalent electric current and magnetic current, using the well-known Green's function approach.

As an ending to this section, it should be noted that both the two types of near-to-far-field transformation are introduced into the FDTD code, in order to get the far-field response of the time modulated array in the time domain, frequency domain, and spatial domain. Moreover, it should also be pointed out that the thin dielectric substrate of the printed dipole is neglected in our FDTD model, since its thickness is much less than the spatial increment (Δx, Δy, and Δz). This will not deteriorate the numerical results greatly and will simplify our numerical model.

4. NUMERICAL RESULTS AND DISCUSSION

In order to validate the accuracy of our FDTD model and to examine the transient response of the time modulated linear arrays, numerical results for the arrays modulated with VAS and BPCM schemes are presented in this section.

The dipole antenna element in the array consists of two arms, with a length of $l = 36.50\,\text{mm}$ and a width of $w = 7.50\,\text{mm}$ for each arm. The size of the ground plane shown in Figure 1 is $L \times W = 1.84\,\text{m} \times 0.40\,\text{m}$, on which the printed dipoles are mounted with an offset of $h = 48.00\,\text{mm}$ from the ground plane. A nonuniform mesh was used herein to ensure the sufficient accuracy while the memory requirements are kept as low as possible. By setting the operating frequency to be 1.56 GHz for the time modulated linear arrays with both VAS and BPCM schemes, the computational domain is then discretized by $97 \times 243 \times 18$ cells, where the increments in the spatial are: $\Delta x = 4.56\,\text{mm}$, $\Delta y = 7.92\,\text{mm}$, $\Delta z = 7.50\,\text{mm}$. The time increment is determined by the Courant Condition [12], which is set to be 10.49 picoseconds in our model. Besides, the Huygens's surface apart from the equipment is set to be quarter of the wavelength at the center frequency. A five-layered PML is used to terminate the mesh to form a radiation boundary condition.

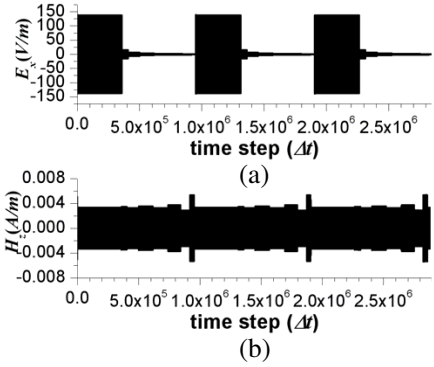

Figure 3. Near-field transient response of the VAS modulated linear array. (a) Transient excitation at the grid of the 1st dipole; (b) transient response on the top face of the Huygens's surface.

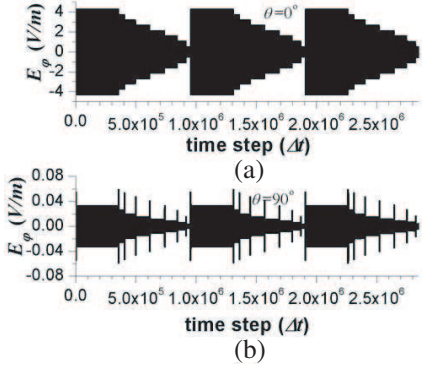

Figure 4. Far-field waveforms of the VAS modulated linear array in the H-plane. (a) $\theta = 0°$; (b) $\theta = 90°$.

We take the linear antenna array modulated with VAS scheme as the first example. The time modulated array with uniform excitation is used to synthesis a -25 dB SLLs discrete Taylor (D-Taylor) pattern with $\bar{n} = 4$. The pulse repetition period $T_p = 10\,\mu$s, implying a modulation frequency of 100 kHz. Figure 3(a) gives the transient excitation signal E_x at the central grid of the 1st dipole, and Figure 3(b) plots the near-field transient response H_z on the top face of the Huygens's surface paralleled to the xoy-plane. It is apparent to see that both of them reveal the periodic attribute of the time modulated arrays. From Figure 3(b), it is also observed that the FDTD updating procedure is stable, and no shock wave has been stirred up during the time evolution.

Illustrated in Figure 4 are the H-plane (yoz-plane) co-polar far-field waveforms at two radiation angles, which are obtained through the time domain near-to-far-field transformation. The envelope of the waveform in the broadside ($\theta = 0°$) and endfire ($\theta = 90°$) directions reflects the fact that the elements in the time modulated VAS array are switched off from two ends of the array by turns in one pulse period, while the elements in the array center are always switched on. Additionally, the physical essence of the VAS can also be found by a comparison between the envelope of waveforms and the diagram of on-off switching time sequence function [10]. To check the validity of the FDTD model, the frequency domain near-to-far-

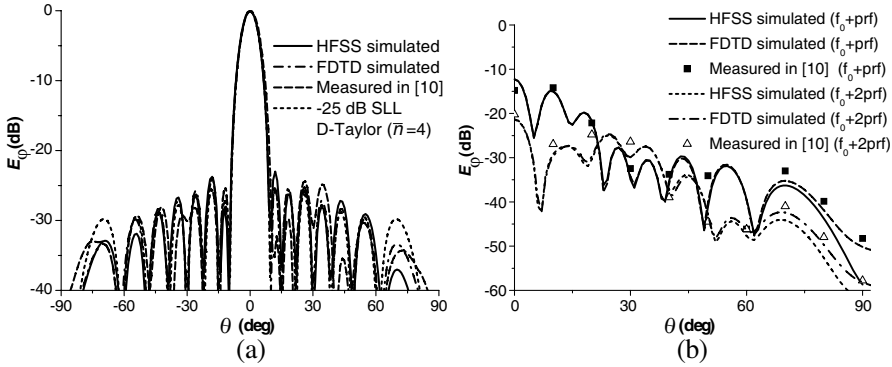

Figure 5. Radiation patterns at the center frequency and the first two sidebands for the VAS modulated linear array. (a) Comparison of the measured radiation patterns with those obtained from FDTD simulation and HFSS simulation at the center frequency; (b) comparison of the measured radiation patterns in [10] with those obtained from FDTD simulation and HFSS simulation at the first two sidebands.

field transformation is applied to the near-field data to obtain the far-field pattern. Figure 5(a) shows the FDTD simulated normalized co-polar radiation pattern in the H-plane at the center frequency f_0, in comparison with the measured pattern and radiation patterns simulated using the commercial software HFSS in [11]. Figure 5(a) also shows the target pattern of a -25 dB discrete Taylor ($\bar{n} = 4$) pattern. As can be seen, the FDTD simulated pattern, HFSS simulated pattern, and the measured pattern in [10] are in good agreement, and they are all close to the target -25 dB discrete Taylor pattern. The FDTD simulated relative SLL is -25.27 dB, which is close to the HFSS simulated SLL of -22.98 dB and measured SLL of -23.92 dB. Shown in Figure 5(b) are the FDTD simulated radiation patterns at the first two sideband frequencies, the measured results [10] and results obtained from the HFSS simulation [11] are also presented for comparison. As can be seen, the simulated results obtained from the FDTD method and the commercial software HFSS are in good agreement, and both of the two groups of simulated results are in reasonable agreement with the measured patterns.

As the second example, the FDTD method is employed to analyze the time modulated linear antenna array with BPCM time scheme. The continuous time modulation (C-Scheme) is introduced, and the number of the consecutive "on" elements at each time instant is

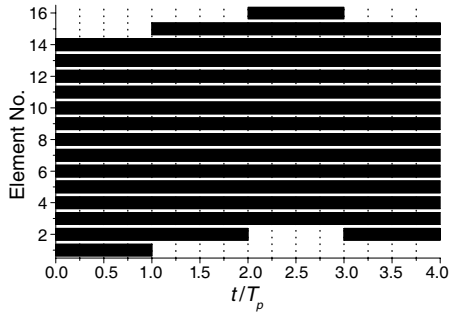

Figure 6. Time sequences of a 16-element linear array with C-scheme BPCM ($M = 14$).

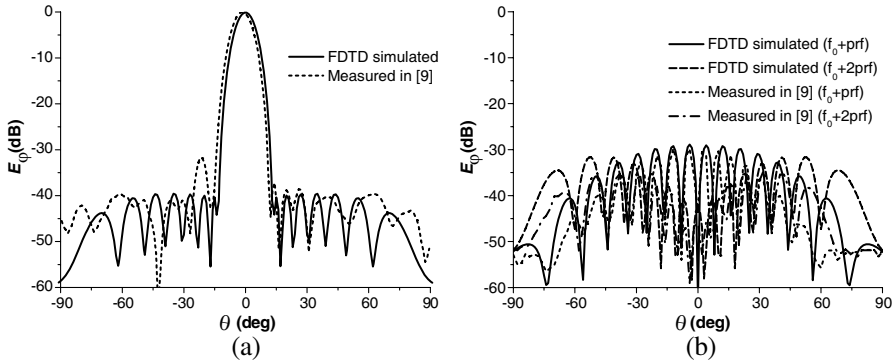

Figure 7. Comparison of the measured radiation patterns in [9] with those obtained from FDTD simulation for the 16-element linear array with C-scheme BPCM ($M = 14$). (a) Comparison at the center frequency; (b) comparison at the first two sidebands.

selected as $M = 14$. The static excitation $A_k\,(k = 1, 2, \ldots, N)$ with a dynamic range ratio of 3.8 was accepted to synthesize a -40 dB SLL D-Taylor pattern ($\bar{n} = 7$) at the center frequency f_0. The pulse repetition frequency *prf* is set to be 1.0 MHz, which is a higher *prf* than that in the first example, implying less time steps are required in one pulse repetition period. Thus the running time consumed in this example decreased greatly. The time sequence diagram for the array is shown in Figure 6. The FDTD simulated radiation patterns at the center frequency and the first two sidebands are shown in Figure 7, and the measured radiation patterns in [9] are also presented in Figure 7. It is observed that the FDTD simulated radiation patterns are close to those of the measured results. The FDTD simulated SLL of the radiation pattern at the center frequency is -39.6 dB, close to the target value of

−40 dB, but the deviation from the measured SLL is slightly large and this may be due to the measurement error in our experiment system. Moreover, it is found that there is also relatively large deviation between the simulation and measurement results. However, the FDTD simulations agree well with those simulated in [9]. Therefore, we can conclude that measured pattern at center frequency may be inaccurate, and the accuracy of FDTD simulations is also demonstrated. The FDTD simulated maximum sideband level is −28.9 dB, which is in good agreement with the measured value of −29.9 dB.

The good agreement between the FDTD simulated results (Figure 5 and Figure 7) and those accurate measured data or simulation results from other methods demonstrates that the neglect of the thin dielectric substrate in our FDTD model is valid. Figure 8 shows the FDTD simulated 3-D space and frequency response plot. The two branches split from the sidelobes in the frequency domain have not been separated completely. This can also be observed from the time sequence diagram in Figure 6, where the number of moving elements is large, leading to a very small Doppler frequency shift at the positive and negative θ directions.

Thirdly, in order to investigate the Doppler frequency shift effect of time modulated linear arrays with BPCM scheme in time domain, the FDTD method is again employed to analyze a time modulated linear antenna array with C-Scheme BPCM and a smaller number of moving elements. The number of the consecutive "on" elements at each time instant is selected as $M = 6$. The static excitation A_k $(k = 1, 2, \ldots, N)$ with a dynamic range ratio of 1.75 was adopted

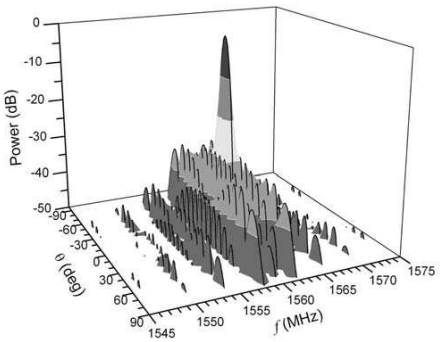

Figure 8. Space and frequency response for the 16-element linear array with C-scheme BPCM ($M = 14$).

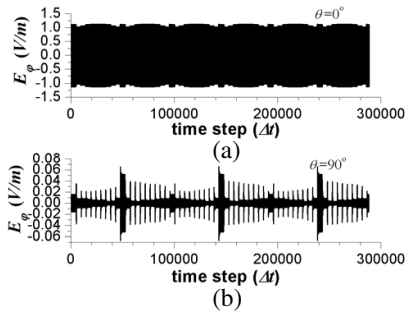

Figure 9. Far-field waveforms for the 16-element linear array with C-scheme BPCM ($M = 6$). (a) $\theta = 0°$; (b) $\theta = 90°$.

to synthesize a $-40\,\mathrm{dB}$ SLL D-Taylor pattern ($\bar{n} = 7$) at the center frequency f_0, with $T_p = 1.0\,\mu\mathrm{s}$ and $prf = 1.0\,\mathrm{MHz}$. We consider the far-field response of the BPCM modulated linear antenna array in the time domain, frequency domain, and spatial domain. Figure 9 presents the waveforms of the co-polar field in the directions of $\theta = 0^\circ$ and $\theta = 90^\circ$ in the H-plane, which are obtained by the time domain transformation. Again, the periodicity of the modulated array is found, and a stable updating procedure is hold on when the time marches on. By applying a quadrature demodulation technique to the far-field signals shown in Figure 9 and the far-field signal in the direction of $\theta = 10^\circ$, the obtained instantaneous phases of the far-field waveforms at the three directions are plotted in Figure 10. The instantaneous frequency is defined as:

$$f_{ins} = C \cdot \frac{d\phi}{dt} \tag{11}$$

where C is a constant coefficient. Figure 10(a) compares the instantaneous phases of the waveforms at $\theta = 0^\circ$ and $\theta = 10^\circ$. It can be seen that there is no Doppler frequency shifting in the direction of $\theta = 0^\circ$, which is the maximum radiation direction in the linear array. However, when the observation angle is away from the broadside, the amount of Doppler frequency shifting in that direction increases. As can been seen from Figure 10(b), the amount of frequency shifting increases distinctively from $\theta = 10^\circ$ to $\theta = 90^\circ$. In order to investigate the impact of the Doppler frequency shifting on the radiation pattern, the 3-D spatial and frequency response obtained through the frequency domain transformation is given in Figure 11. It can be observed

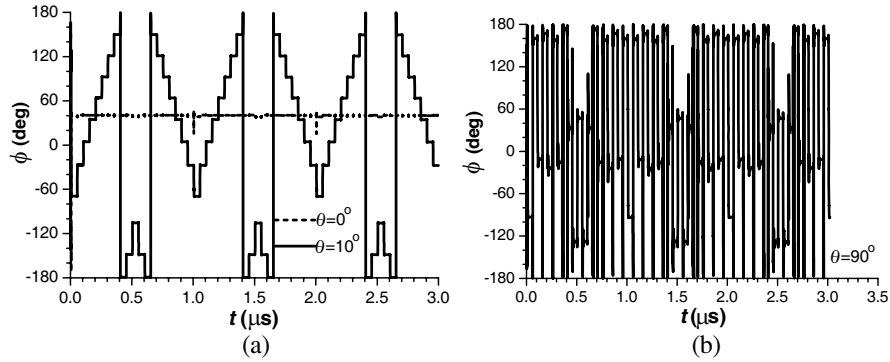

Figure 10. Instantaneous phases of waveforms at three different radiation angles. (a) Comparison of the instantaneous phases in the directions of $\theta = 0^\circ$ and $\theta = 10^\circ$; (b) instantaneous phases in the direction of $\theta = 90^\circ$.

that the sidelobes experienced both the upper and lower frequency shifting, similar to those observations in [9]. Additionally, the 3-D response in Figure 11 can be further examined in another two different perspectives. The first one is that due to the impact of the Doppler frequency shifting, the two branches were markedly split from the sidelobes at the center frequency and are distributed at several sidebands, due to the relatively smaller number of moving elements. The Doppler frequency shifting thus leads to a lower SLLs at the center frequency than those in conventional arrays. Another one is that the two sidelobe branches are distributed at frequencies far away from the center frequency, especially for BPCM with a higher moving speed. Thus, the bandwidth of the radar passband is extended. The same observations were also obtained in [9] by analytical method, which validates the correctness of the FDTD model in this study. Consequently, the FDTD method provides an attractive tool for the analysis of the transient response of the time modulated arrays, and the Doppler frequency shifting in BPCM array can be interpreted thoroughly with respect to the instantaneous phases.

Finally, the H-plane normalized co-polar radiation patterns at the center frequency and the first two sidebands are also presented in Figure 12. The normalized radiation pattern recovered at the center frequency is close to the target -40 dB D-Taylor pattern. A front-to-back ratio of 25 dB is obtained for this time modulated array, due to the conducting ground plane.

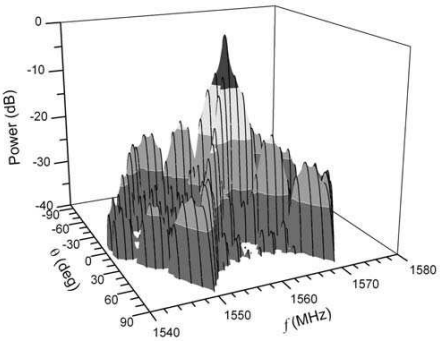

Figure 11. Space and frequency response for the 16-element linear array with C-scheme BPCM ($M = 6$).

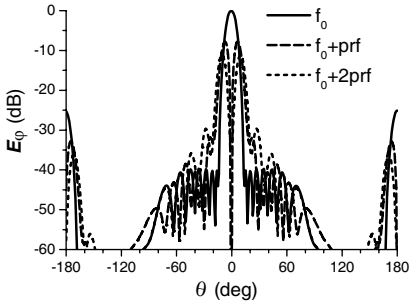

Figure 12. Radiation patterns at the center frequency and the first two sidebands for the linear array with C-scheme BPCM ($M = 6$).

5. CONCLUSION

Full-wave simulations for time modulated linear antenna arrays with VAS and C-BPCM schemes have been carried out using the FDTD method. In order to get a full understanding of the arrays modulated with the two time sequences, the far-field transient responses are presented, with which the physical essence of the two time sequences are well explained. Furthermore, the radiation patterns are computed using the frequency domain transformation. Through comparison with the measured results and results obtained from other full-wave simulation method, the accuracy and validity of the FDTD method in the simulation of the time modulated linear arrays are demonstrated. Other time modulated arrays are also of necessity to be simulated in the time domain, and it is hoped that the proposed FDTD method can be an attractive tool for the analysis of time modulated arrays.

ACKNOWLEDGMENT

This work was supported by the Natural Science Foundation of China under Grant (60971030), the New Century Excellent Talent Program in China under Grant (NCET-06-0809), and was also partially supported by the 111 Project of China under Grant (B07046).

REFERENCES

1. Kummer, W. H., A. T. Villeneuve, T. S. Fong, and F. G. Terrio, "Ultra-low sidelobes from time-modulated arrays," *IEEE Trans. Antennas Propagat.*, Vol. 11, No. 5, 633–639, Nov. 1963.
2. Yang, S., Y. B. Gan, and A. Qing, "Sideband suppression in time modulated linear arrays by the differential evolution algorithm," *IEEE Antennas and Wireless Propagat. Lett.*, Vol. 1, 173–175, Dec. 2002.
3. Yang, S., Y. B. Gan, and P. K. Tan, "Comparative study of low sidelobe time modulated linear arrays with different time schemes," *Journal of Electromagnetic Waves and Applications*, Vol. 18, No. 11, 1443–1458, Nov. 2004.
4. Yang, S., "Study of low sidelobe time modulated linear antenna arrays at millimeter-waves," *International Journal of Infrared and Millimeter-waves*, Vol. 26, No. 3, 443–456, Mar. 2005.
5. Yang, S., Y. B. Gan, and P. K. Tan, "A new technique for power pattern synthesis in time modulated linear arrays," *IEEE Antennas and Wireless Propagat. Lett.*, Vol. 2, 285–287, Dec. 2003.

6. Yang, S., Y. B. Gan, A. Qing, and P. K. Tan, "Design of a uniform amplitude time modulated linear array with optimized time sequences," *IEEE Trans. Antennas Propagat.*, Vol. 53, No. 7, 2337–2339, Jul. 2005.
7. Yang, S. and Z. Nie, "A review of the four dimensional antenna arrays," *J. Electron. Sci. Tech. China*, Vol. 4, No. 3, 193–201, Sep. 2006.
8. Yang, S., Y. B. Gan, and A. Qing, "Moving phase center antenna arrays with optimized static excitations," *Microwave and Optical Tech. Lett.*, Vol. 38, No. 1, 83–85, Jul. 2003.
9. Yang, S., Y. B. Gan, and P. K. Tan, "Linear antenna arrays with bidirectional phase center motion," *IEEE Trans. Antennas Propagat.*, Vol. 53, No. 5, 1829–1835, May 2005.
10. Yang, S. and Z. Nie, "Mutual coupling compensation in time modulated linear antenna arrays," *IEEE Trans. Antennas Propagat.*, Vol. 53, No. 12, 4182–4185, Dec. 2005.
11. Zhu, X., S. Yang, and Z. Nie, "Full-wave simulation of time modulated linear antenna arrays in frequency domain," *IEEE Trans. Antennas Propagat.*, Vol. 56, No. 5, 1479–1482, May 2008.
12. Yee, K. S., "Numerical solution of initial boundary value problems involving Maxwell's equations in isotropic media," *IEEE Trans. Antennas Propagat.*, Vol. 14, No. 8, 302–307, May 1966.
13. Lei, J.-Z., C.-H. Liang, W. Ding, and Y. Zhang, "EMC analysis of antennas mounted on electrically large platforms with parallel fdtd method," *Progress In Electromagnetics Research*, PIER 84, 205–220, 2008.
14. Yun, Z. and M. F. Iskander, "Implementation of floquet boundary conditions in FDTD analysis of periodic phased array antennas with skewed grid," *Electromagnetics*, Vol. 20, No. 5, 445–452, 2000.
15. Berenger, J. P., "A perfectly matched layer for the absorption of electromagnetic waves," *J. Comput. Phys.*, Vol. 114, No. 2, 185–200, 1994.
16. Berenger, J. P., "Three-dimensional perfectly matched layer for the absorption of electromagnetic waves," *J. Comput. Phys.*, Vol. 127, No. 2, 363–379, 1996.
17. Yee, K. S., D. Ingham, and K. Shlager, "Time-domain extrapolation to the far field based on FDTD calculations," *IEEE Trans. Antennas Propagat.*, Vol. 39, No. 3, 410–413, Mar. 1991.
18. Luebbers, R. J., K. S. Kunz, M. Schneider, and F. Hunsberger, "A finite-difference time-domain near zone to far zone transforma-

tion," *IEEE Trans. Antennas Propagat.*, Vol. 39, No. 4, 429–433, Apr. 1991.

19. Reineix, A. and B. Jecko, "Analysis of microstrip patch antennas using finite difference time domain method," *IEEE Trans. Antennas Propagat.*, Vol. 37, No. 11, 1361–1369, Nov. 1989.
20. Umashankar, K. R. and A. Taflove, "A novel method to analyze electromagnetic scattering of complex objects," *IEEE Trans. Electromagn. Compat.*, Vol. 24, No. 24, 397–405, Nov. 1982.
21. Taflove, A. K., R. Umashankar, and T. G. Jurgens, "Validation of FD-TD modeling of the radar cross section of three-dimensional structures spanning up to nine wavelengths," *IEEE Trans. Antennas Propagat.*, Vol. 33, No. 6, 662–666, Jun. 1985.